



# Optimized removal process and tailored adsorption mechanism of crystal violet and methylene blue dyes by activated carbon derived from mixed orange peel and watermelon rind using microwave-induced ZnCl<sub>2</sub> activation

Nurul Afiqah Mohd Hanafi<sup>1</sup> · Ahmed Saud Abdulhameed<sup>2,3</sup> · Ali H. Jawad<sup>1</sup> · Zeid A. ALOthman<sup>4</sup> · Tarek A. Yousef<sup>5</sup> · O. K. Al Duaij<sup>5</sup> · Norah Salem Alsaari<sup>6</sup>

Received: 22 August 2022 / Revised: 2 December 2022 / Accepted: 5 December 2022  
© The Author(s), under exclusive licence to Springer-Verlag GmbH Germany, part of Springer Nature 2022

## Abstract

Releasing wastewater containing organic dyes into water bodies generates a variety of hazards for humans and marine life. Thus, developing effective adsorbents to remove organic dyes from wastewater is critical. Herein, a mixture of the orange peel (OP) and watermelon rind (WR) wastes was converted into a mesoporous activated carbon (OPWRAC) via microwave-induced ZnCl<sub>2</sub>. Several analytical techniques such as XRD, N<sub>2</sub> adsorption–desorption isotherms, FTIR, pH<sub>pzc</sub>, and SEM–EDX were applied to characterize the physicochemical properties of OPWRAC. Subsequently, the adsorptive efficiency of OPWRAC was comprehensively explored towards the removal of two structurally different organic dyes, namely, crystal violet (CV) and methylene blue (MB). The operational adsorption conditions such as OPWRAC dose (0.04–0.1 g) coded as (A), solution pH (4–10) coded as (B), and contact time (10–60 min) coded as (C) were statistically optimized using the response surface methodology-Box-Behnken design (RSM-BBD). The adsorption isotherm data for CV and MB dyes agree with the Freundlich model, and the kinetic data can be explained by the pseudo-second-order model. Thus, OPWRAC displays remarkable adsorption capacity for capturing CV (137.8 mg/g) and MB (200.7 mg/g). The tailored adsorption mechanism of CV and MB by the OPWRAC indicates the involvement of several types of electrostatic forces,  $\pi$ - $\pi$  stacking, pore filling, and H-bonding. The output of this research shows the feasibility of converting the mixture of OP and WR into promising activated carbon with potential application for capturing two structurally cationic dyes from an aqueous environment.

**Keywords** Orange peel · Watermelon rind · Activated carbon · Microwave · Crystal violet · Methylene blue

✉ Ali H. Jawad  
ali288@uitm.edu.my; ahjm72@gmail.com

<sup>1</sup> Faculty of Applied Sciences, Universiti Teknologi MARA, 40450 Shah Alam, Selangor, Malaysia

<sup>2</sup> Department of Medical Instrumentation Engineering, Al-Mansour University College, Baghdad, Iraq

<sup>3</sup> College of Engineering, University of Warith Al-Anbiyaa, Karbala, Iraq

<sup>4</sup> Chemistry Department, College of Science, King Saud University, Riyadh 11451, Saudi Arabia

<sup>5</sup> Department of Chemistry, Science College, Imam Mohammad Ibn Saud Islamic University (IMSIU), P.O. Box 90950, Riyadh 11623, Saudi Arabia

<sup>6</sup> Department of Chemistry, College of Science, Princess Nourah bint Abdulrahman University, P. O. Box 84428, 11671 Riyadh, Saudi Arabia

## 1 Introduction

Water pollution is a globally observed phenomenon due to its negative effects on the ecosystem and human health. Water pollution is generated from discharging effluents related to industrial activities into freshwater without treatment [1]. Organic dyes (e.g., methylene blue (MB), crystal violet (CV)) are one the significant constituents of industrial effluents and considered one of the common water pollutants due to their harmful effects on the environment and human health, for instance, rapid heartbeat, nausea, mental confusion, shortness of breath, skin irritation, and diminishing photosynthesis [2, 3]. Therefore, it is crucial that organic dyes are removed from industrial wastewater. Organic dyes are typically removed from water using a variety of techniques, including ion exchange [4], electrochemical

degradation [5], photocatalysis [6], adsorption [7], and coagulation/flocculation [8]. Most of these procedures are hindered by secondary waste, cost, or difficulty. The adsorption method has been identified as the optimum way to separate these contaminants owing to its amazing properties such as non-susceptibility to contaminants, reusability, lower waste production, low cost, and high efficiency [9].

Activated carbon (AC) has special characteristics, for instance, porosity, greater surface area, adsorption ability, plenty of functional groups, and thermal stability [10]. These characteristics make it an effective adsorbent in adsorption techniques to remove organic dyes [11]. However, commercial AC has a number of drawbacks, such as producing from nonrenewable precursors and high costs, which limit its applicability [12]. The availability of affordable and sustainable precursors is itself a major obstacle to the production of AC. In order to prepare AC from plentiful, affordable, ecological, and sustainable precursors, research efforts have increased [13]. Due to its renewability, availability, economic efficiency, and nontoxicity, the production of AC from lignocellulosic materials constitutes a viable option [14]. Numerous earlier literatures have reported the generation of AC using different lignocellulosic precursors, for instance, mango peels and seed wastes [15], *Aesculus hippocastanum* L. biomass [16], orange peel [17], hawthorn kernel [18], and *Althaea officinalis* L. [19].

Typically, a number of methods, including traditional pyrolysis and microwave radiation, can be used to create AC from lignocellulosic biomass [20]. The microwave heating approach used in this study has several benefits over conventional heating, including a large amount of desired product, improved heating efficiency, process control, and consistent heat distribution [21]. In the synthesis of AC, precursors are impregnated with activating chemicals (e.g.,  $\text{ZnCl}_2$ ,  $\text{H}_3\text{PO}_4$ ,  $\text{KOH}$ , and  $\text{K}_2\text{CO}_3$ ), and carbonization and activation take place concurrently [22]. Among various chemical activators,  $\text{ZnCl}_2$  promotes fabricating AC with outstanding properties like pore volume, smaller pore size, and higher surface area, increasing the carbon yield, and plentiful reactive groups for the uptaking of pollutants [23]. Lately, generating AC from a variety of precursors using  $\text{ZnCl}_2$  as an effective chemical agent has been reported and the resultant AC has been successfully used to remove contaminants such as methylene blue dye [24], tetracycline hydrochloride [25], Cr (VI) ion [23], nitrate [26], and malachite green dye [27].

The goal of this study is to produce high-surface-area activated carbon (hereinafter, termed OPWRAC) from sustainable and affordable precursors (orange peels (OP), watermelon rind (WR)) via microwave-induced  $\text{ZnCl}_2$  activation. The generated OPWRAC was used to remove CV and MB dyes from aqueous systems. Box-Behnken design (BBD) was selected to establish the optimal conditions for CV and MB adsorption onto the OPWRAC surface. Kinetic and

isotherm models were used to simulate the empirical adsorption data of the CV and MB dyes. A probable mechanism for the CV and MB adsorption on OPWRAC was outlined.

## 2 Materials and methods

### 2.1 Materials

The fruit biomass wastes orange peel (OP) and watermelon rind (WR) as a precursor of activated carbon were collected from fruit bars in Shah Alam city, Selangor state, Malaysia. For the adsorption study, the stranded solutions (1000 mg/L) for CV ( $\lambda_{\text{max}}$ , 584 nm; MW, 408 g/mol; R&M Chemicals) and MB ( $\lambda_{\text{max}}$ , 661 nm; MW, 319.86 g/mol; R&M Chemicals) were prepared and adjusted as needed. In all experiments, analytical-grade chemicals and reagents from R&M Chemicals, Malaysia, including hydroxide sodium (NaOH) pellets, zinc chloride ( $\text{ZnCl}_2$ ), sodium chloride (NaCl) powder, and hydrochloric acid (HCl) were supplied without additional purification.

### 2.2 OPWRAC preparation

The fruit biomass wastes (OP and WR) were thoroughly cleaned with hot distilled water to remove dust and other unwanted substances. Prior to the drying process by an oven, the samples (orange peel and watermelon rind) were left few days under sunlight for air-drying process. Then, the drying process using an oven was carried out at 100 °C for 24 h to remove the remaining moisture and to ensure a perfect drying process for the precursors. After that, the OPWR was crashed into powder form and sieved to uniform particles size (2 mm). In the activation process, 1 g of the precursor (OPWR, the mixing ratio of OP and WR was 1:1) and 2 g of chemical activator ( $\text{ZnCl}_2$ ) were mixed at a fixed impregnation ratio of 1:2 (this mixing ratio was predetermined to be the optimum mixing ratio). In this regard, it was proven in the literatures that the best impregnation mixing ratio of biomass wastes such as carrot juice pulp and pomegranate peel [7] and mango peels and seeds [15] with  $\text{ZnCl}_2$  chemical activator was 1:2 by using a microwave activation technique. Subsequently, the OPWR/ $\text{ZnCl}_2$  system was then heated for 24 h at 100 °C inside an oven to achieve complete drying. Thus, the activated OPWR was transferred to a specially designed microwave oven (SAM-SUNG ME711K, 20 L) before being subjected to the microwave irradiation (800 W) for 20 min under pure  $\text{N}_2$  (99.99%) condition with a fixed flow rate of 100 mL/min (pre-identified as the optimum activation settings). After that, distilled water was used to wash the resultant OPWRAC to neutralize the pH of the solution. For drying purpose, the produced OPWRAC was placed inside an oven for 24 h at 100 °C. Then, the OPWRAC was sieved using 250- $\mu\text{m}$  sieve to obtain a uniform

particle size (250 μm), and it was then kept in a sealed container for subsequent use.

### 2.3 Characterization

The OPWRAC’s surface physical properties, such as its specific surface area and pore volume, were analyzed using the equipment (Micromeritics, ASAP 2060). Scanning electron microscopy (SEM, Zeiss Supra 40 VP) and energy dispersive X-ray (EDX) examination were used to characterize the surface topologies and the mineral composition of the OPWRAC before and after the adsorption of CV and MB. Using an X-ray polycrystal diffractometer (XRD, PANalytical X’Pert PRO), the crystalline nature of OPWRAC was examined in the 10–90° scanning range. All samples were examined between 4000 and 450 cm<sup>-1</sup> using Fourier transform infrared (FTIR) spectra acquired from an FTIR spectrometer (Perkin-Elmer, Spectrum RX I) to characterize fundamental groups of OPWR and OPWRAC before and after the adsorption of CV and MB. A point of zero charge (pH<sub>pzc</sub>) method was employed to identify the charge of the OPWRAC surface [28].

### 2.4 Experimental design

For the optimization process, a Box-Behnken design (BBD) was used together with quadratic programming to determine the optimal operational conditions for CV and MB removal by OPWRAC within 3 input parameters (OPWRAC dose, solution pH, and time). The software Design Expert (13.0, Stat-Ease, USA) was used to construct the adsorption study and statistically interpret of the results. Table 1 illustrates 3 ranges (i.e., -1, 0, and +1) of explored factors, namely, OPWRAC dose (A), solution pH (B), and time (C). The preliminary tests were used to determine the coded values of the parameters as well as the parameters to be employed in the adsorption optimization. The second-degree polynomial employed for fitting the components (independent factors and MB removal) of the model is illustrated in Eq. (1).

$$Y = \beta_0 + \sum \beta_i X_i + \sum \beta_{ii} X_i^2 + \sum \sum \beta_{ij} X_i X_j \quad (1)$$

where *Y* is reply;  $\beta_i$  is linear impact;  $\beta_{ij}$  is interaction impact;  $\beta_0$  is intercept; and  $X_i$  and  $X_j$  are independent variables. The data of developed models along with responses

**Table 1** Codes and actual variables and their levels in BBD

Codes	Variables	Level 1 (-1)	Level 2 (0)	Level 3 (+1)
A	OPWRAC dose (g)	0.04	0.07	0.1
B	Solution pH	4	7	10
C	Time (min)	10	35	60

(CV removal (%) and MB removal (%)) are given in Table 2. The adsorption study of the CV and MB was carried out by adding a specific dose of adsorbent to Erlenmeyer flasks containing 100 mL of the dye solution before being placed inside a thermostatic water bath shaker at a fixed shaking speed of 110 strokes per min. Then, adsorbent-free liquids were produced by passing the mixtures in a 0.45-μm Nylon syringe filter. The concentration of the CV and MB during the treatment process was spectrophotometrically assessed at  $\lambda_{max} = 661$  nm and at  $\lambda_{max} = 584$  nm, respectively, using a spectrophotometer (HACH DR 3900). Then, the dye removal efficiency (*R*, %) of CV and MB dyes was determined by using Eq. (2).

$$R \% = \frac{(C_o - C_e)}{C_o} \times 100 \quad (2)$$

where  $C_o$  (mg/L) and  $C_e$  (mg/L) represent the concentrations of the adsorbates (CV and MB) in their initial and equilibrium states, respectively.

### 2.5 Adsorption study of CV and MB by OPWRAC

The adsorption study of the MB and CV dyes onto the surface of OPWRAC was carried out in batch mode at the following operational conditions: OPWRAC dosage (0.1 g), solution pH (10), and time (35 min). These operational conditions were found to be the best conditions to achieve the highest removal of CV (91.6%) and MB (94.1%), according

**Table 2** Experimental matrix based on BBD approach for designing experiments and corresponding quadratic model response

Run	A: dose (g)	B: pH	C: time (min)	CV removal (%)	MB removal (%)
1	0.04	4	35	38.6	52.7
2	0.1	4	35	70.8	88.9
3	0.04	10	35	51.1	69.8
4	0.1	10	35	91.6	94.1
5	0.04	7	10	30.3	52.2
6	0.1	7	10	58.5	81.6
7	0.04	7	60	49.7	65.2
8	0.1	7	60	89.4	91.4
9	0.07	4	10	34.9	62.8
10	0.07	10	10	53.1	79.3
11	0.07	4	60	62.1	77.1
12	0.07	10	60	82.7	84.9
13	0.07	7	35	70.8	82.3
14	0.07	7	35	72.7	79.7
15	0.07	7	35	72.6	77.7
16	0.07	7	35	72.5	78.6
17	0.07	7	35	77.9	79.3

to the BBD model (run no. 4 in Table 2). Thus, the adsorption equilibrium experiments were conducted with these optimum input variables throughout a range (20–200 mg/L) of starting CV and MB concentrations. The same methodology outlined in the Sect. 2.4 was used to carry out batch adsorption testing for MB and CV dyes. The following mathematical formula (3) was applied to calculate the equilibrium adsorption quantity ( $q_e$ , mg/g) of the OPWRAC:

$$q_e = \frac{(C_o - C_e)V}{W} \quad (3)$$

where  $W$  (g) represents the OPWRAC's weight and  $V$  (L) refers to the volume of the dye solution.

### 3 Results and discussion

#### 3.1 Characterization of OPWRAC

The surface area and porosity of the OPWRAC are necessary aspects in the adsorption of CV and MB dyes. The specific surface area and pore properties of OPWRAC are stated in Table 3. According to calculations, OPWRAC's total pore volume and specific surface area are 0.49 cm<sup>3</sup>/g and 661.3 m<sup>2</sup>/g, respectively. This finding (total pore volume) indicates the formation of pores during the activation procedure with the chemical agent ZnCl<sub>2</sub> [23]. According to IUPAC [29], the OPWRAC has a mesoporous structure with pores ranging in size from 2.0 to 50 nm, as demonstrated by the findings of the mean pore diameter (4.57 nm). The N<sub>2</sub> adsorption/desorption isotherms of the OPWRAC are displayed in Fig. 1 together with the related BJH (Barrett, Joyner, Halenda) pore size distributions (insert). The isotherms show that the OPWRAC has a mesoporous structure since they match the type-IV isotherm [29]. Additionally, the BJH desorption curve demonstrated that the OPWRAC had a broad pore width distribution in the mesoporous region. The hysteresis loop seen in Fig. 1 could be categorized as type H4, revealing the presence of mesopores in the OPWRAC structure [30]. The fact that ZnCl<sub>2</sub> and its hydrates had minuscule particle sizes may help to explain why most of the holes created in

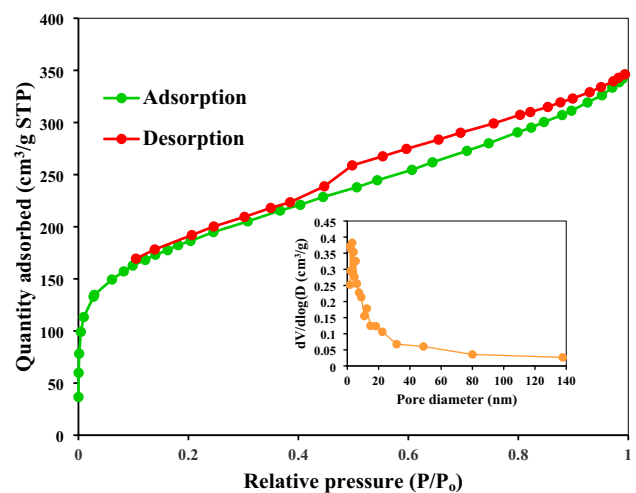


Fig. 1 The N<sub>2</sub> adsorption–desorption isotherms and pore size distribution of OPWRAC

the OPWRAC prepared with the ZnCl<sub>2</sub> agent were quite small [31]. In this respect, high surface area and porous activated carbon materials were produced from biomass wastes such as carrot juice pulp and pomegranate peel (1202.2 m<sup>2</sup>/g) [7] and mango peels and seeds (1151.6 m<sup>2</sup>/g) [15] using microwave-assisted ZnCl<sub>2</sub> activation. According to the above data, the obtained OPWRAC possesses a great degree of porosity, a significant pore volume, and a sizable specific surface area; it provides a considerable number of active sites which may bind with CV and MB molecules effectively.

In order to figure out the phase structure of OPWRAC, XRD analysis was utilized. The XRD pattern of OPWRAC is presented in Fig. 2. A broad peak at  $2\theta$  of 24° and a sharp peak at  $2\theta$  of 44.2° in the XRD pattern

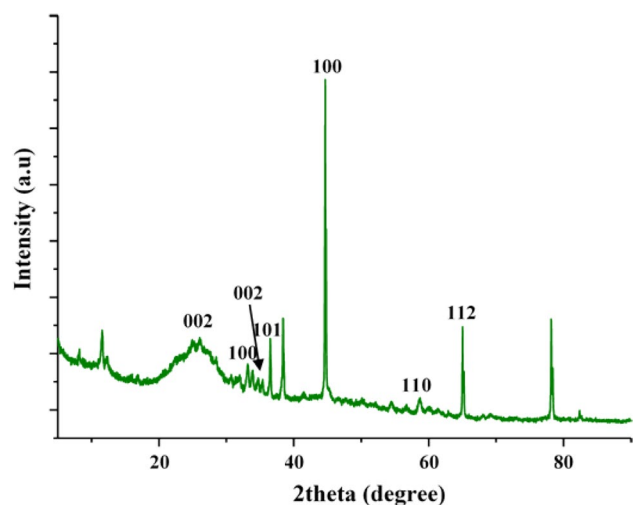


Fig. 2 XRD pattern OPWRAC

Table 3 Surface properties of OPWRAC

Parameter(s)	Value
BET surface area (m <sup>2</sup> /g)	661.3 m <sup>2</sup> /g
Langmuir surface area (m <sup>2</sup> /g)	912.1 m <sup>2</sup> /g
Total volume in pores (cm <sup>3</sup> /g)	0.49 cm <sup>3</sup> /g
Pore diameter (nm)	4.57 nm



of OPWRAC were associated with the (002) and (100) reflection planes of the graphitic structure of OPWRAC, respectively [32]. It can also be demonstrated that OPWRAC displays significant peaks at  $2\theta=31.9^\circ$  (100),  $34.5^\circ$  (002),  $36.3^\circ$  (101),  $56.7^\circ$  (110), and  $66.5^\circ$  (112), which are related to the action of an activator ( $\text{ZnCl}_2$ ) during the production of OPWRAC and correlate to ZnO (JCPDS file no. 01-079-0205) [33].

To gain knowledge about the functional groups present in the OPWR, OPWRAC, OPWRAC-CV, and OPWRAC-MB, FTIR spectroscopic analysis was employed. In Fig. 3, the FTIR spectra of OPWR, OPWRAC, OPWRAC-CV, and OPWRAC-MB are exhibited. The OPWR spectrum (Fig. 3a) exhibits absorption bands in the  $3300\text{--}3800\text{ cm}^{-1}$  range, which is ascribed to the O-H stretching vibrations of the cellulose, hemicellulose, pectin, and lignin [34]. Various peaks were also noticed at  $2923\text{ cm}^{-1}$ ,  $2341\text{ cm}^{-1}$ ,  $1650\text{ cm}^{-1}$ ,  $1450\text{ cm}^{-1}$ , and  $1027\text{ cm}^{-1}$ , which are ascribed to the C-H vibrations in  $-\text{CH}_3$  and  $-\text{CH}_2-$  groups, alkyne group ( $\text{C}\equiv\text{C}$ ), carbonyl  $\text{C}=\text{O}$  groups, stretching vibration of  $\text{C}=\text{C}$  band, and C-O stretching, respectively [34, 35].

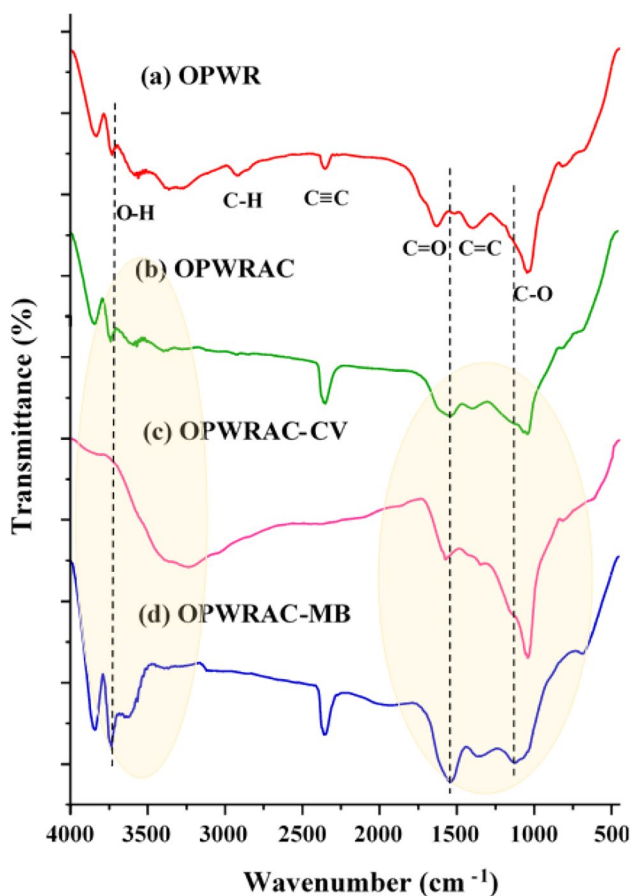


**Fig. 3** FTIR spectra of **a** OPWR, **b** OPWRAC, **c** OPWRAC-CV, and **d** OPWRAC-MB

Comparing the FTIR spectra of OPWRAC to OPWR reveals modifications or shifts in the strength of several peaks, demonstrating the decomposition of surface groups throughout the carbonization and activation steps. The FTIR spectra of OPWRAC-CV (following CV adsorption on the OPWRAC surface) and OPWRAC-MB (following MB adsorption on the OPWRAC surface) showed spectra that were relatively similar to OPWRAC with significant alterations in several bands, demonstrating that the OPWRAC's functional groups participated in the adsorption of CV and MB.

SEM-EDX analysis was used to analyze the morphological characteristics and elemental constitution of OPWRAC, OPWRAC-CV, and OPWRAC-MB. The findings of the SEM images and EDX assessments for OPWRAC, OPWRAC-CV, and OPWRAC-MB are illustrated in Fig. 4a-c. According to Fig. 4a, the surface of OPWRAC is uneven, diverse, and rough. The results of the EDX analysis of OPWRAC show that C, O, and N elements are present. After the adsorption of CV (Fig. 4b) and MB (Fig. 4c), the morphological structure of OPWRAC was dramatically changed into a smoother one in line with the adsorption of CV and MB species on the OPWRAC surface. C, O, and N are present in the EDX data for OPWRAC-CV, whereas C, O, N, and S are present in the EDX data for OPWRAC-MB. The S element's existence is linked to the composition of the MB dye.

### 3.2 Statistical evaluation

ANOVA test was used to analyze the connection between the predicted and empirical data and the finesse of the derived second-order mathematical model. The outcomes of the ANOVA for MB removal are mentioned in Table S1. The  $F$ -values of the CV removal and MB removal were 102.27 and 110.55, respectively, stating the possibility of employing the model for assessing the relation between the analyzed and experimental data [36]. The models' relevance and the fact that the calculated and observed removal data of CV and MB dyes are fully consistent were outlined by the high  $R^2$  values of CV dye removal ( $R^2=0.99$ ) and MB dye removal (0.99). The developed models are also logical because the deviations between the adjusted  $R^2$  (0.98 for both CV and MB removal models) and predicted  $R^2$  (0.95 for CV removal model and 0.96 for MB removal model) values were 0.03 and 0.02, respectively [37]. The expected models' validity was confirmed by the negligible  $p$  values (lack of fit), which were 0.7641 and 0.6982 for CV removal and MB removal, respectively [37]. The characteristics of the proposed model are presumed to be statistically relevant if  $p < 0.05$  and vice versa. The following codes A, B, C, AC,  $A^2$ ,  $B^2$ , and

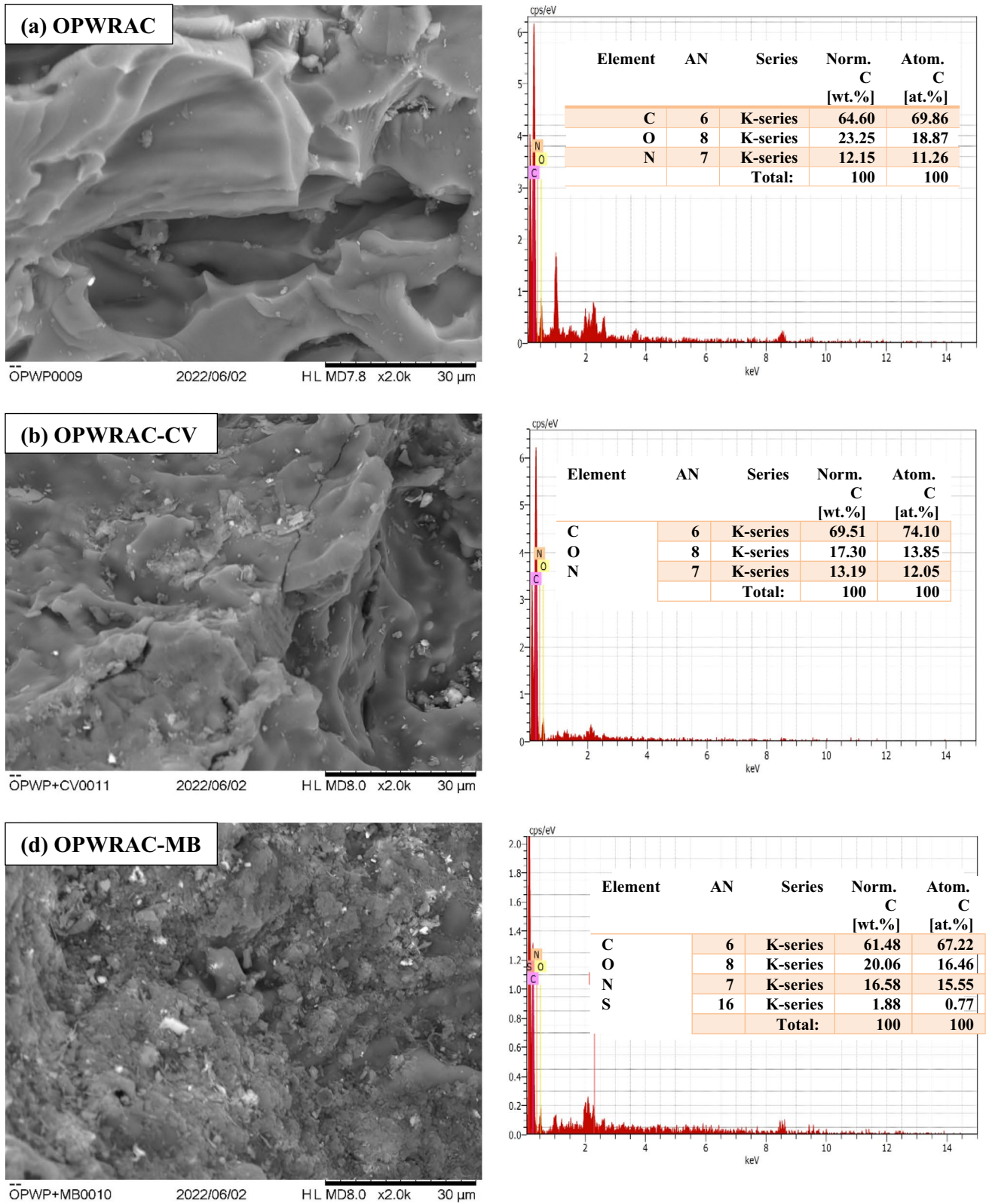


Fig. 4 SEM images and EDX spectra of a OPWRAC and b OPWRAC-CV, and c OPWRAC-MB

$C^2$  are considered statistically influencing CV removal, whereas the following codes A, B, C, AB, BC,  $A^2$ , and  $C^2$  are considered statistically influencing MB removal. By estimating the most significant input variables, the quadratic Eqs. (4, 5) of the CV removal and MB removal were created.

$$\text{CV removal (\%)} = +73.30 + 17.57A + 9.01B + 13.39C + 2.88AC - 5.75A^2 - 4.53B^2 - 10.58C^2 \tag{4}$$

$$\text{MB removal (\%)} = +79.52 + 14.51A + 5.83B + 5.34C - 2.98AB - 2.17BC - 3.29A^2 + 0.14B^2 - 3.63C^2 \tag{5}$$

The normal probability of the CV removal and MB removal models, respectively, is shown as graphs in Fig. S1a and b. The dots (Fig. S1a and b) appear to be

tightly fitted with the single line, highlighting that the model and the ANOVA findings are adequate and acceptable [38]. It also can be concluded from Fig. S1(a, b) that the residuals are independent. The diagrams show that the relationship between the predicted and actual values of CV and MB dye removal are outlined in Fig. S1c and

d. The strong correlation between the observational outcomes (CV removal and MB removal) and those that are theoretically estimated is clearly seen in Fig. S1c and

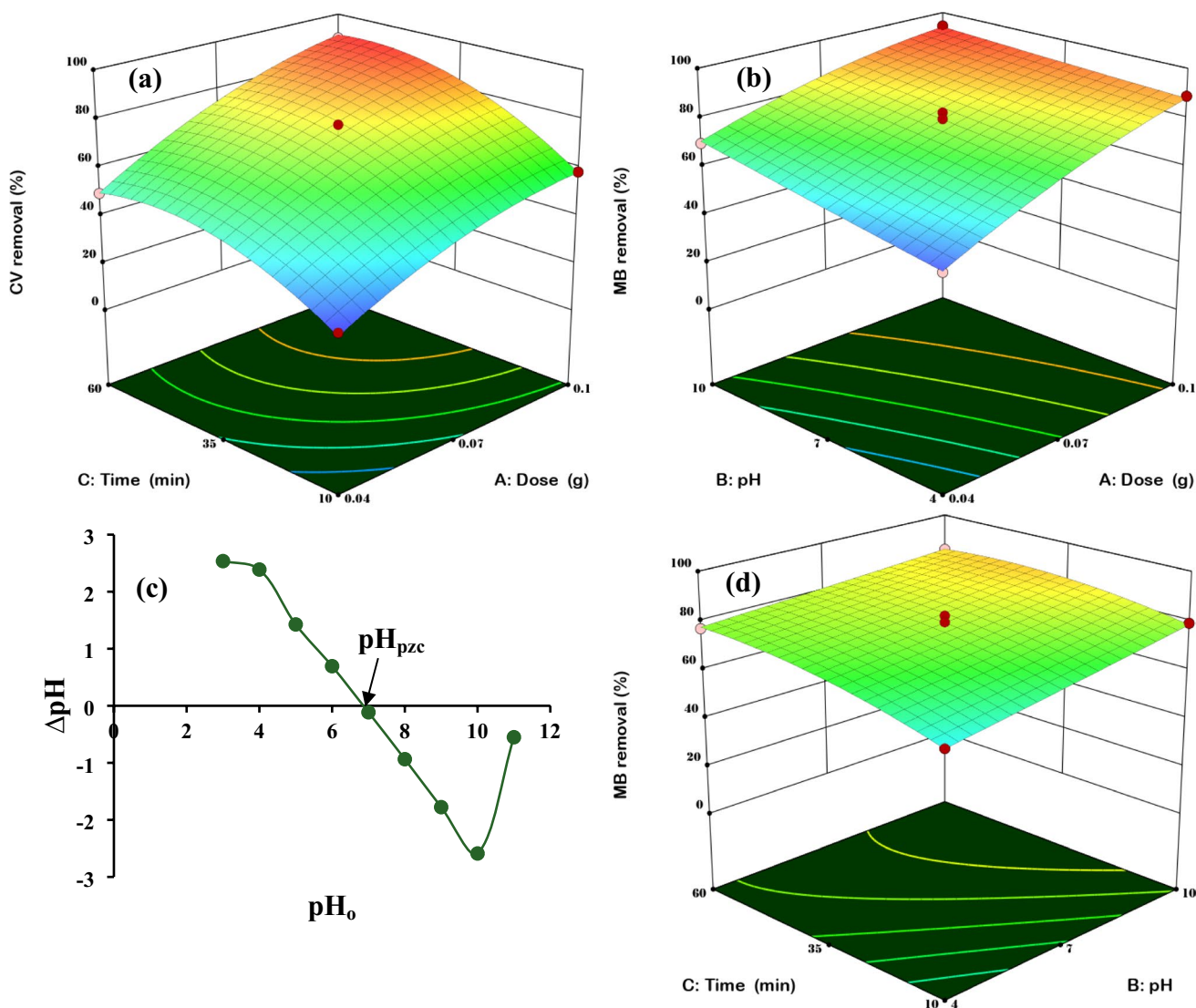


**Fig. 5** 3D response surface plots of significant interactions including **a** AC (OPWRAC dose×time) for CV removal, **b** AB (OPWRAC dose×pH) for MB removal, and **c** BC (time×pH) for MB removal, while **d** pH<sub>pzc</sub> of OPWRAC

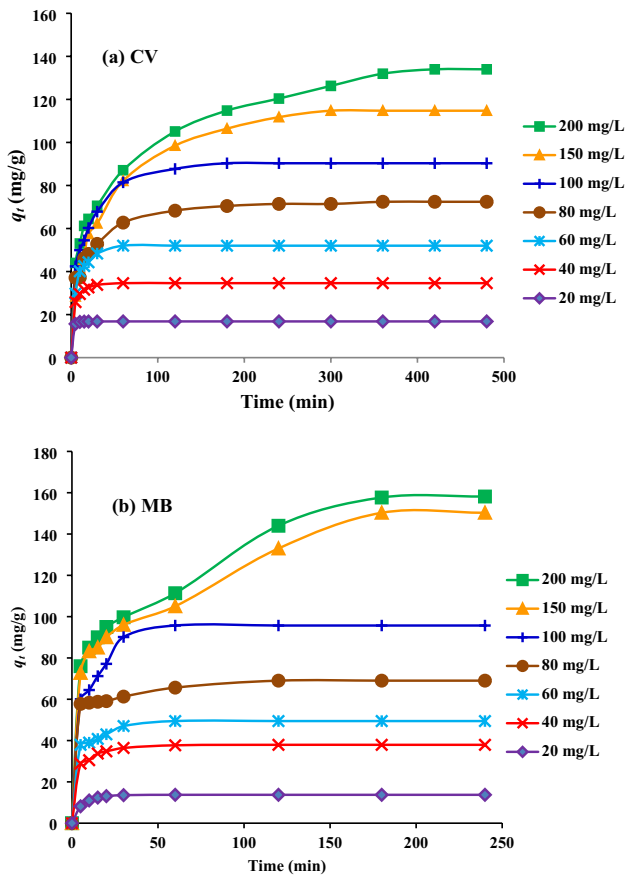


**Fig. 6** Effect of the contact time on **a** CV and **b** MB adsorption at several concentrations (dosage=0.1 g, solution pH=10, temperature=25 °C, agitation speed=85 rpm, and volume of solution=100 mL)

d, demonstrating the validity of the constructed models from the statistical perspective.

### 3.3 Dual effects of variables

3D response surface curves were generated to evaluate the influence of the input variables and to identify the key interactions between the input variables on the CV and MB removal processes. The dual effect of

the OPWRAC dose and time on the CV removal rate is shown in Fig. 5a (3D plot), while the pH (7) was maintained constant. The results shown in Fig. 5a show that increasing the OPWRAC dose from 0.04 g to 0.1 g improved the removal efficiency of MB. Thus, this trend is caused by excessive surface area and effective adsorption sites of OPWRAC with higher OPWRAC doses. The magnitude of CV removal increased with higher time (60) according to Fig. 5a. This is a result of the CV molecules needing enough time to pass into the OPWRAC pores and bind on the OPWRAC surface and reaching to the equilibrium time.

The dual effect of the OPWRAC dose and pH on the MB removal rate is shown in Fig. 5b, while the time (35 min) was maintained constant. From the findings displayed in Fig. 5b, the adsorption effectiveness of MB was greatly enhanced at pH 10. In this regard, the  $pH_{pzc}$  characteristic of OPWRAC and the preferred type (anionic or cationic) of the MB to OPWRAC surface may be used to analyze the influence of pH on MB adsorption. The  $pH_{pzc}$  of OPWRAC was 6.9, as shown in Fig. 5c. As a result, at a high basic pH value (10) above  $pH_{pzc}$ , the OPWRAC surface and MB dye molecules are negatively and positively charged. As a result, as shown in the formula below, this amplifies OPWRAC's attention to binding positively charged MB molecules and enhances MB dye absorption (6).



The dual effect of the pH and time on the MB removal rate is shown in Fig. 5d, while the OPWRAC dose (0.07 g) was maintained constant. Figure 5d demonstrates that the OPWRAC's adsorption effectiveness of the MB dye was very close at different adsorption times (10–60 min). This observation is related to the fact that the OPWRAC's active sites were mainly occupied at 35 min.

### 3.4 Adsorption study

The adsorption capacity of the OPWRAC is influenced by changing the initial concentration (20–200 mg/L) of

**Table 4** Adsorption kinetics and isotherm nonlinear models

Models	Formula	Descriptions
Pseudo-first order (PFO)	$q_t = q_e(1 - e^{-k_1 t})$	$k_1$ , pseudo-first-order rate constant (1/min)
Pseudo-second order (PSO)	$q_t = \frac{q_e^2 k_2 t}{1 + q_e k_2 t}$	$k_2$ , pseudo-second-order rate constant (g/mg min)
Langmuir	$q_e = \frac{q_m K_L C_e}{1 + K_L C_e}$	$q_m$ , monolayer capacity (mg/g) $K_L$ , Langmuir constant (L/mg)
Freundlich	$q_e = K_F C_e^{1/n}$	$K_F$ , Freundlich constant (mg/g) (L/mg) <sup>1/n</sup> $n$ , adsorption intensity
Temkin	$q_e = \frac{RT}{b_T} \ln(K_T C_e)$	$K_T$ , Temkin constant (L/mg) $b_T$ , adsorption intensity (J/mol)



**Table 5** PFO and PSO kinetic parameters for the CV and MB adsorption on OPWRAC

CV concentration (mg/L)	$q_{e \text{ exp}}$ (mg/gm)	PFO			PSO		
		$q_{e \text{ cal}}$ (mg/gm)	$K_1$ (1/min)	$R^2$	$q_{e \text{ cal}}$ (mg/gm)	$k_2 \times 10^{-2}$ (g/mg min)	$R^2$
20	16.83	16.80	0.5368	0.99	16.90	18.630	0.99
40	34.60	34.13	0.2479	0.99	35.02	1.6590	0.99
60	52.02	51.244	0.1451	0.98	53.08	0.5244	0.99
80	71.42	69.457	0.0736	0.92	72.88	0.1661	0.97
100	90.33	88.159	0.0701	0.95	92.43	0.1240	0.98
150	114.74	110.13	0.0332	0.96	120.39	0.0362	0.99
200	133.98	121.867	0.0375	0.90	132.54	0.0381	0.96
MB Concentration (mg/L)	$q_{e \text{ exp}}$ (mg/gm)	PFO			PSO		
		$q_{e \text{ cal}}$ (mg/gm)	$K_1$ (1/min)	$R^2$	$q_{e \text{ cal}}$ (mg/gm)	$k_2 \times 10^{-2}$ (gm/mg min)	$R^2$
20	13.72	13.655	0.1711	0.99	14.35	2.2773	0.99
40	37.93	36.61	0.2556	0.97	38.33	1.3618	0.99
60	49.44	46.965	0.2581	0.95	49.56	0.9656	0.98
80	69.009	64.068	0.4229	0.96	66.94	1.2240	0.98
100	95.703	92.869	0.1305	0.94	98.29	0.2384	0.98
150	150.28	130.40	0.0790	0.82	142.66	0.0796	0.91
200	158.16	138.92	0.0745	0.83	151.95	0.0706	0.92

the CV and MB solutions, as shown in Fig. 6a and b. During this experiment, 0.1 g of OPWRAC adsorbent was used, and the solution pH was set at 10. As a result of increasing the initial CV and MB concentration from 20 to 200 mg/L, the adsorption capacity of OPWRAC was dramatically increased (16.83 to 133.98 mg/g for CV; 13.72 to 158.16 mg/g for MB). This observation can be assigned to the relatively high concentration gradient, which boosts dye mobility inside the OPWRAC's internal pores and causes the dye to transfer to the effective surface of the OPWRAC [39].

### 3.5 Adsorption kinetics

The scale-up and technological development of adsorptive removal of CV and MB utilizing OPWRAC benefit greatly from the data given by the kinetic analysis. The investigational adsorption data were used to assess kinetic models such as pseudo-first order [40] and pseudo-second order [41]. Table 4 shows the formulae for each of these models, whereas Table 5 offers the kinetic parameter data. It was found that the relatively high  $R^2$  values (see Table 5) appeared in the PSO model rather than the PFO model and the calculated values of  $q_e$  for the PSO kinetic model were remarkably similar to the experimental values of  $q_e$ , indicating that the PSO model can reasonably explain the adsorption of CV and MB on the OPWRAC. This result denotes that CV and MB adsorption is attributed to the chemisorption process resulting from the interactions between the cationic groups of CV and MB with the anionic groups of OPWRAC [42].

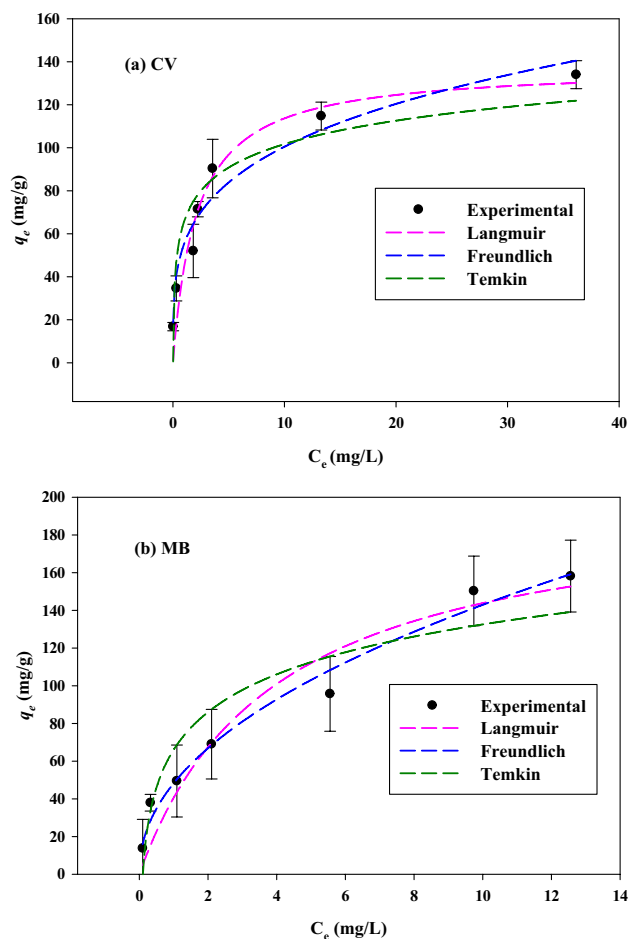


**Fig. 7** Adsorption isotherms of **a** CV and **b** MB onto OPWRAC (dosage=0.1 g, solution pH=10, temperature=25 °C, agitation speed=85 rpm, and volume of solution=100 mL)

**Table 6** The parameters of isotherm models and equilibrium parameters for CV and MB adsorption on OPWRAC

Adsorption isotherm	Parameter	CV	MB
Langmuir	$q_m$ (mg/gm)	137.8	200.7
	$K_a$ (L/mg)	0.47	0.25
	$R^2$	0.93	0.94
Freundlich	$K_f$ (mg/gm) (L/mg) <sup>1/n</sup>	55.1	48.2
	$n$	3.83	2.11
	$R^2$	0.95	0.98
Temkin	$K_T$ (L/mg)	4.16	2.28
	$b_T$ (J/mol)	157.6	85.7
	$R^2$	0.89	0.88

### 3.6 Adsorption isotherms

Adsorption isotherms were used to assess the nature of interfacial contact between the CV/MB molecules and OPWRAC surface and the OPWRAC's maximal adsorptive capacity. The adsorption of CV and MB on OPWRAC was explored in-depth with the Langmuir [43], Freundlich [44], and Temkin [45] isotherms. The formula for every one of these models is described in Table 4. As indicated in Table 7 and Fig. 7a and b, parameters and diagrams of isotherm models were generated and reported. The Freundlich model is well-matched with the empirical adsorption data of CV and MB based on the  $R^2$  values depicted in Table 6. This finding illustrates that the CV and MB molecules were adsorbed as a multilayer on the heterogeneous surface of the OPWRAC [46]. Additionally, 137.8 mg/g and 200.7 mg/g are the determined adsorption capacities of OPWRAC towards CV and MB, respectively. The reported adsorption capacities of OPWRAC and other adsorbents for CV and MB adsorption are shown in Table 7. The findings demonstrate the possibility and applicability of converting the fruit biomass wastes into mesoporous activated carbon (OPWRAC) with highly preferable adsorptive capacity towards various cationic dyes.

**Table 7** Comparison of the adsorption capacity of OPWRAC towards CV and MB dyes with different ACs

Adsorbents	Dye	$q_{max}$ (mg/g)	References
OPWRAC	CV	137.8	This study
OPWRAC	MB	200.7	This study
African star apples whole seed activated carbon	CV	251.0	[47]
Zinc oxide nanorods loaded on activate carbon	CV	113.64	[48]
Activated carbon from poultry litter	CV	70.32	[49]
Activated carbon prepared from lemon wood	CV	23.6	[50]
Activated carbon from tea waste	MB	357.14	[51]
Activated carbon from pineapple crown	MB	292	[52]
Banana stem-based activated carbon	MB	101.01	[53]
Apricot stone activated carbon	MB	88.50	[54]

### 3.7 Tailored adsorption mechanism of CV and MB dyes

The key interactions listed in the literature as leading to the adsorption of organic dyes on activated carbons include electrostatic interaction, pore-filling,  $\pi$ - $\pi$  interaction, and hydrogen bonding [55]. These interactions may all be involved in the adsorption process of CV and MB by OPWRAC as shown in Fig. 8. The electrostatic interactions between the CV and MB cations and the negatively charged surface of the OPWRAC considerably accelerated the CV and MB adsorption process at a pH higher than the  $pH_{pzc}$  of the OPWRAC, indicating that this parameter constituted a feasible path for CV and MB adsorption onto the OPWRAC. The interaction of nitrogen atoms of adsorbates (CV and MB) with free hydrogen atoms of adsorbent (OPWRAC) produces H-bonding interactions, which contribute to the adsorption of the CV and MB dyes. Furthermore, based on BET and SEM examinations of the OPWRAC, which supports its mesoporous structure, CV and MB molecules have molecular sizes of 1.4 nm and 1.43 nm [32, 56], respectively, and may potentially occupy the mesopores in the OPWRAC structure. Lastly, CV and MB contain an aromatic backbone that interacts with OPWRAC's hexagonal structure to make  $\pi$ - $\pi$  stacking.

## 4 Conclusion

A mesoporous activated carbon (OPWRAC) was successfully produced from lignocellulosic biomass (OP and WR) wastes via microwave-induced  $ZnCl_2$  activation at microwave irradiation (800 W) for 20 min with a constant ratio of impregnation (1 g OPWR:2 g  $ZnCl_2$ ). The BBD model identified that the combinations of the OPWRAC dose (0.1 g), pH (10), and time (35 min) resulted in the highest removal of CV (91.6%) and MB (94.1%). The adsorption process of CV and MB dyes was multilayer adsorption,

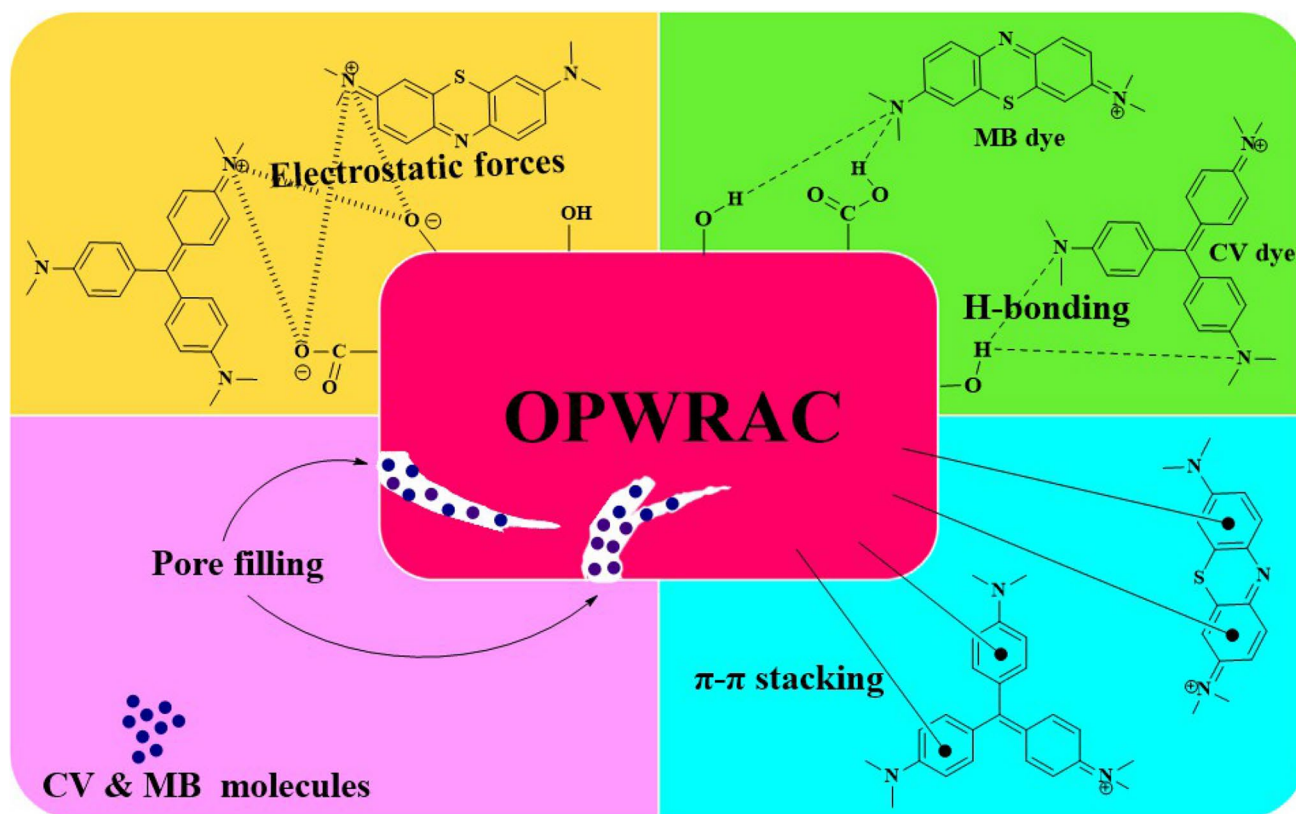


**Fig. 8** Illustration of the possible interaction among OPWRAC and dyes (CV and MB) including electrostatic forces, pore filling, hydrogen bonding, and  $\pi$ - $\pi$  stacking

and it happens via the chemisorption route, according to the kinetic and equilibrium data of CV and MB. Thus, OPWRAC shows remarkable adsorption capacity towards both CV (137.8 mg/g) and MB (200.7 mg/g). Furthermore, the CV and MB adsorption by the OPWRAC is controlled by several mechanisms, comprising electrostatic forces,  $\pi$ - $\pi$  stacking, pore filling, and H-bonding. This study reveals that the OPWRAC synthesized from OP and WR has the possibility to be a promising adsorbent for the treatment of dye-containing effluents.

**Supplementary Information** The online version contains supplementary material available at <https://doi.org/10.1007/s13399-022-03646-z>.

**Author contribution** Nurul Afiqah Mohd Hanafi: formal analysis, validation, data curation. Ahmed Saud Abdulhameed: formal analysis, validation, data curation, and writing original draft. Ali H. Jawad: conceptualization, methodology, software, supervision, project administration, writing, reviewing, and editing. Zeid A. AlOthman: formal analysis and validation. Tarek A. Yousef: validation and funding acquisition. O.K. Alduaijd: formal analysis and funding acquisition. Norah Salem Alsaari: funding acquisition and validation.

**Funding** The authors extend their appreciation to the Deanship of Scientific Research at Imam Mohammad Ibn Saud Islamic University (IMSIU) for funding and supporting this work through Research Partnership Program no. RP-21-09-73. The author (Norah Salem Alsaari)

would like to thank for the support given by Princess Nourah bint Abdulrahman University Researchers Supporting Project Number PNURSP2022R19, Princess Nourah bint Abdulrahman University, Riyadh, Saudi Arabia.

**Data availability** The datasets used and/or analyzed during the current study are available from the corresponding author on reasonable request.

## Declarations

**Ethics approval** Not applicable.

**Consent to participate** Not applicable.

**Consent for publication** Not applicable.

**Competing interests** The authors declare no competing interests.

## References

1. Wang Z, Zhang Y, Kang S, Yang L, Shi H, Tripathee L, Gao T (2021) Research progresses of microplastic pollution in freshwater systems. *Sci Total Environ* 795:148888–148899
2. Tian T, Liu M, Li Y, Han J, Ren L, Lorenz H, Chen J (2022)  $\beta$ -Cyclodextrin carbon-based nanoparticles with a core-shell-shell

- structure for efficient adsorption of crystal violet and bisphenol A. *Particuol* 62:88–97
3. Temel F, Turkyilmaz M, Kucukcongar S (2020) Removal of methylene blue from aqueous solutions by silica gel supported calix [4] arene cage: investigation of adsorption properties. *Eur Polym J* 125:109540–109551
  4. Zaharia MM, Vasiliu AL, Trofin MA, Pamfil D, Bucatariu F, Racovita S, Mihai M (2021) Design of multifunctional composite materials based on acrylic ion exchangers and CaCO<sub>3</sub> as sorbents for small organic molecules. *React Funct Polym* 166:104997–105012
  5. de Toledo WDMC, Pinheiro RA, Trava-Airoldi VJ, Corat EJ (2022) Development of boron-doped diamond (BDD) deposited on carbon nanotubes (CNT) to form BDD/CNT structures relevant for electrochemical degradation. *Diamond Relat Mater* 127:109159–1109170
  6. Jawad AH, Nawi MA (2012) Characterizations of the photocatalytically-oxidized cross-linked chitosan-glutaraldehyde and its application as a sub-layer in the TiO<sub>2</sub>/CS-GLA bilayer photocatalyst system. *J Polym Environ* 20(3):817–829
  7. Suhaimi A, Abdulhameed AS, Jawad AH, Yousef TA, AlDuaij OK, AlOthman ZA, Wilson LD (2022) Production of large surface area activated carbon from a mixture of carrot juice pulp and pomegranate peel using microwave radiation-assisted ZnCl<sub>2</sub> activation: an optimized removal process and tailored adsorption mechanism of crystal violet dye. *Diamond Relat Mater* 130:109456–109467
  8. Ihaddaden S, Aberkane D, Boukerroui A, Robert D (2022) Removal of methylene blue (basic dye) by coagulation-flocculation with biomaterials (bentonite and *Opuntia ficus indica*). *J Water Process Eng* 49:102952–102964
  9. Reshadi MAM, Bazargan A, McKay G (2020) A review of the application of adsorbents for landfill leachate treatment: focus on magnetic adsorption. *Sci Total Environ* 731:138863–138878
  10. Koyuncu F, Güzel F, İnal İİG (2022) High surface area and supermicroporous activated carbon from capsicum (*Capsicum annum L.*) industrial processing pulp via single-step KOH-catalyzed pyrolysis: production optimization, characterization and its some water pollutants removal and supercapacitor performance. *Diamond Relat Mater* 124:108920–108933
  11. Sultana M, Rownok MH, Sabrin M, Rahaman MH, Alam SN (2022) A review on experimental chemically modified activated carbon to enhance dye and heavy metals adsorption. *Clean Eng Technol* 6:100382–100396
  12. Jahan K, Singh V, Mehrotra N, Rathore K, Verma V (2021) Development of activated carbon from KOH activation of pre-carbonized chickpea peel residue and its performance for removal of synthetic dye from drinking water. *Biomass Conv Bioref* <https://doi.org/10.1007/s13399-021-01938-4>.
  13. Gayathiri M, Pulingam T, Lee KT, Sudesh K (2022) Activated carbon from biomass waste precursors: factors affecting production and adsorption mechanism. *Chemosphere* 294:133764–133776
  14. Hoang AT, Kumar S, Lichtfouse E, Cheng CK, Varma RS, Senthilkumar N, Nguyen XP (2022) Remediation of heavy metal polluted waters using activated carbon from lignocellulosic biomass: an update of recent trends. *Chemosphere* 302:134825–134848
  15. Razali NS, Abdulhameed AS, Jawad AH, AlOthman ZA, Yousef TA, Al-Duaij OK, Alsaiani NS (2022) High-surface-area-activated carbon derived from mango peels and seeds wastes *via* microwave-induced ZnCl<sub>2</sub> activation for adsorption of methylene blue dye molecules: statistical optimization and mechanism. *Mol. 27(20):6947–6965*
  16. Isinkaralar K, Gullu G, Turkyilmaz A (2022) Experimental study of formaldehyde and BTEX adsorption onto activated carbon from lignocellulosic biomass. *Biomass Conver Bio* <https://doi.org/10.1007/s13399-021-02287-y>
  17. Jimoh OS, Ibrahim AO, Bello OS (2022) Metformin adsorption onto activated carbon prepared by acid activation and carbonization of orange peel. *Int J Phyto* <https://doi.org/10.1080/15226514.2022.2064815>
  18. Zhen XT, Yu YL, Shi MZ, Zhu SC, Yan TC, Yue ZX, Cao J (2022) Activated carbon derived from hawthorn kernel waste for rapid adsorption of fungicides. *Surf Interfaces* 28:101700–101713
  19. Isinkaralar K (2022) High-efficiency removal of benzene vapor using activated carbon from *Althaea officinalis L.* biomass as a lignocellulosic precursor. *Environ Sci Pollut Res* 29:66728–66740
  20. Rashidi NA, Chai YH, Ismail IS, Othman MFH, Yusup S (2022) Biomass as activated carbon precursor and potential in supercapacitor applications. *Biomass Conver. Bio* <https://doi.org/10.1007/s13399-022-02351-1>
  21. Hijab M, Parthasarathy P, Mackey HR, Al-Ansari T, McKay G (2021) Minimizing adsorbent requirements using multi-stage batch adsorption for malachite green removal using microwave date-stone activated carbons. *Chem Eng Process-Process Intensif* 167:108318–108329
  22. Şahin Ö, Saka C, Ceyhan AA, Baytar O (2015) Preparation of high surface area activated carbon from *Elaeagnus angustifolia* seeds by chemical activation with ZnCl<sub>2</sub> in one-step treatment and its iodine adsorption. *Sep Sci Technol* 50(6):886–891
  23. Luo X, Cai Y, Liu L, Zeng J (2019) Cr (VI) adsorption performance and mechanism of an effective activated carbon prepared from bagasse with a one-step pyrolysis and ZnCl<sub>2</sub> activation method. *Cellulose* 26(8):4921–4934
  24. Yağmur HK, Kaya İ (2021) Synthesis and characterization of magnetic ZnCl<sub>2</sub>-activated carbon produced from coconut shell for the adsorption of methylene blue. *J Mol Struct* 1232:130071–130083
  25. Cai Y, Liu L, Tian H, Yang Z, Luo X (2019) Adsorption and desorption performance and mechanism of tetracycline hydrochloride by activated carbon-based adsorbents derived from sugar cane bagasse activated with ZnCl<sub>2</sub>. *Molecules* 24(24):4534–4551
  26. Nassar H, Zyoud A, El-Hamouz A, Tanbour R, Halayqa N, Hilal HS (2020) Aqueous nitrate ion adsorption/desorption by olive solid waste-based carbon activated using ZnCl<sub>2</sub>. *Sustain Chem Pharm* 18:100335–100344
  27. Jayabalakrishnan RM, Maheswari M, Boomiraj K, Oumabady S (2021) Coconut shell derived ZnCl<sub>2</sub> activated carbon for malachite green dye removal. *Water Sci Technol* 83(5):1167–1182
  28. Dalvand A, Nabizadeh R, Ganjali MR, Khoobi M, Nazmara S, Mahvi AH (2016) Modeling of Reactive Blue 19 azo dye removal from colored textile wastewater using L-arginine-functionalized Fe<sub>3</sub>O<sub>4</sub> nanoparticles: optimization, reusability, kinetic and equilibrium studies. *J Magnet Magnet Mater* 404:179–189
  29. Sing KS (1985) Reporting physisorption data for gas/solid systems with special reference to the determination of surface area and porosity (Recommendations 1984). *Pure Appl Chem* 57(4):603–619
  30. Saygılı H, Güzel F (2016) High surface area mesoporous activated carbon from tomato processing solid waste by zinc chloride activation: process optimization, characterization and dyes adsorption. *J Clean Prod* 113:995–1004
  31. Goncalves M, Castro CS, Boas IK, Soler FC, Pinto EDC, Lavall RL, Carvalho WA (2019) Glycerin waste as sustainable precursor for activated carbon production: adsorption properties and application in supercapacitors. *J Environ Chem Eng* 7(3):103059–103070
  32. Dao MU, Le HS, Hoang HY, Tran VA, Doan VD, Le TTN, Sirotkin, (2021) A Natural core-shell structure activated carbon beads derived from *Litsea glutinosa* seeds for removal of methylene blue: facile preparation, characterization, and adsorption properties. *Environ Res* 198:110481–110493
  33. Hadi S, Taheri E, Amin MM, Fatehizadeh A, Lima EC (2021) Fabrication of activated carbon from pomegranate husk by dual



- consecutive chemical activation for 4-chlorophenol adsorption. *Environ Sci Pollut Res* 28(11):13919–13930
34. Köseoğlu E, Akmil-Başar C (2015) Preparation, structural evaluation and adsorptive properties of activated carbon from agricultural waste biomass. *Adv Powder Technol* 26(3):811–818
  35. Masoudian N, Rajabi M, Ghaedi M (2019) Titanium oxide nanoparticles loaded onto activated carbon prepared from bio-waste watermelon rind for the efficient ultrasonic-assisted adsorption of Congo red and phenol red dyes from wastewaters. *Polyhedron* 173:114105–114114
  36. Jawad AH, Abdulhameed AS, Wilson LD, Hanafiah MAKM, Nawawi WI, ALOthman ZA, Rizwan Khan M (2021) Fabrication of Schiff's base chitosan-glutaraldehyde/activated charcoal composite for cationic dye removal: optimization using response surface methodology. *J. Polym. Environ.* 29(9):2855–2868
  37. Kutluay S, Temel F (2021) Silica gel based new adsorbent having enhanced VOC dynamic adsorption/desorption performance. *Colloids Surf A: Physicochem Eng Asp* 609:125848–125862
  38. Marichamy MK, Kumaraguru A, Jonna N (2021) Particle size distribution modeling and kinetic study for coagulation treatment of tannery industry wastewater at response surface optimized condition. *J Clean Prod* 297:126657–126673
  39. Jawad AH, Abdulhameed AS, Hanafiah MAKM, ALOthman ZA, Khan MR, Surip SN (2021) Numerical desirability function for adsorption of methylene blue dye by sulfonated pomegranate peel biochar: modeling, kinetic, isotherm, thermodynamic, and mechanism study. *Korean. J. Chem. Eng.* 38(7):1499–1509
  40. Lagergren S (1898) Zur theorie der sogenannten adsorption gelöster stoffe. *Vet Akad Handl* 24:1–39
  41. Ho YS, McKay G (1998) Sorption of dye from aqueous solution by peat. *Chem Eng J* 70:115–124
  42. Theamwong N, Intarabumrung W, Sangon S, Aintharabunya S, Ngernyen Y, Hunt AJ, Supanchaiyamat N (2021) Activated carbons from waste *Cassia bakeriana* seed pods as high-performance adsorbents for toxic anionic dye and ciprofloxacin antibiotic remediation. *Bioresour Technol* 341:125832–125842
  43. Langmuir I (1918) The adsorption of gases on plane surfaces of glass, mica and platinum. *J Am Chem Soc* 40:1361–1403
  44. Freundlich HMF (1906) Over the adsorption in solution. *J Phys Chem* 57:385–471
  45. Temkin MI (1940) Kinetics of ammonia synthesis on promoted iron catalysts. *Acta physiochim URSS* 12:327–356
  46. Saleem A, Hussain A, Chaudhary A, Ahmad QA, Iqtedar M, Javid A, Muhammad Akram A (2022) Acid hydrolysis optimization of pomegranate peels waste using response surface methodology for ethanol production. *Biomass Conv Bioref* 12:1513–1524
  47. Oni BA, Olawole OC, Ayeni AO, Sanni SE (2020) African star apples whole seed activated carbon powder as a bio-adsorbent of crystal violet dye removal from aqueous solution. *Water Conser Sci Eng* 5(1):97–114
  48. Dil EA, Ghaedi M, Ghaedi A, Asfaram A, Jamshidi M, Purkait MK (2016) Application of artificial neural network and response surface methodology for the removal of crystal violet by zinc oxide nanorods loaded on activate carbon: kinetics and equilibrium study. *J Taiwan Inst Chem Eng* 59:210–220
  49. Yusuff AS, Ajayi OA, Popoola LT (2021) Application of Taguchi design approach to parametric optimization of adsorption of crystal violet dye by activated carbon from poultry litter. *Sci African* 13:00850–0063
  50. Foroutan R, Peighambaroust SJ, Peighambaroust SH, Pateiro M, Lorenzo JM (2021) Adsorption of crystal violet dye using activated carbon of lemon wood and activated carbon/Fe<sub>3</sub>O<sub>4</sub> magnetic nanocomposite from aqueous solutions: a kinetic, equilibrium and thermodynamic study. *Mol* 26(8):2241–2260
  51. Tuli FJ, Hossain A, Kibria AF, Tareq ARM, Mamun SM, Ullah AA (2020) Removal of methylene blue from water by low-cost activated carbon prepared from tea waste: a study of adsorption isotherm and kinetics. *Environ Nanotechnol Monit Manage* 14:100354–100362
  52. da Silva AI, Paranha G, Maia LS, Mulinari DR (2021) Development of activated carbon from pineapple crown wastes and its potential use for removal of methylene blue. *J Nat Fibers* 1–16.
  53. Misran E, Bani O, Situmeang EM, Purba AS (2022) Banana stem based activated carbon as a low-cost adsorbent for methylene blue removal: isotherm, kinetics, and reusability. *Alex Eng J* 61(3):1946–1955
  54. Abbas M, Trari M (2020) Removal of methylene blue in aqueous solution by economic adsorbent derived from apricot stone activated carbon. *Fibers Polym* 21(4):810–820
  55. Mahapatra U, Chatterjee A, Das C, Manna AK (2021) Adsorptive removal of hexavalent chromium and methylene blue from simulated solution by activated carbon synthesized from natural rubber industry biosludge. *Environ Technol Innova* 22:101427–101408
  56. Wathukarage A, Herath I, Iqbal MCM, Vithanage M (2019) Mechanistic understanding of crystal violet dye sorption by woody biochar: implications for wastewater treatment. *Environ Geochem Health* 41(4):1647–1661

**Publisher's note** Springer Nature remains neutral with regard to jurisdictional claims in published maps and institutional affiliations.

Springer Nature or its licensor (e.g. a society or other partner) holds exclusive rights to this article under a publishing agreement with the author(s) or other rightsholder(s); author self-archiving of the accepted manuscript version of this article is solely governed by the terms of such publishing agreement and applicable law.